Powder Technology 195 (2009) 196–202

Contents lists available at ScienceDirect

Powder Technology

journal homepage: www.elsevier.com/locate/powtec

Effect of SiC_p multimodal distribution on pitting behavior of Al/SiC_p composites prepared by reactive infiltration

M. Montoya-Dávila [a], M.I. Pech-Canul [a,*], M.A. Pech-Canul [b]

[a] Cinvestav Saltillo, Carr. Saltillo-Mty Km 13, Saltillo Coah, 25900, Mexico
[b] Cinvestav Mérida, Km. 6 Antigua Carr. a Progreso Apdo. Postal 73, Cordemex, Mérida, Yuc., 97310, Mexico

ARTICLE INFO

Article history:
Received 1 November 2008
Received in revised form 25 March 2009
Accepted 11 June 2009
Available online 27 June 2009

Keywords:
Multimodal particle size distribution
SiC powders
Liquid metal infiltration
Cyclic polarization
Pitting corrosion
Al–Mg–Si alloys

ABSTRACT

The effect of coated-SiC_p multimodal-size-distribution on the pitting behavior of Al/SiC_p composites was investigated. α-SiC powders (10, 54, 86, and 146 μm) were properly mixed and coated with silica to produce porous preforms with 0.6 volume fraction of the reinforcement with monomodal, bimodal, trimodal, and cuatrimodal size distribution. The preforms were infiltrated with the alloy Al–13 Mg–1.8Si (wt.%) in argon followed by nitrogen at 1100 °C for 60 min. The composites were characterized by X-ray diffraction (XRD) and scanning electron microscopy (SEM) before and after cyclic polarization measurements in 0.1 M NaCl de-aerated solutions. Results show that whereas corrosion and passivation potentials are not influenced with increase in SiC_p particle size distribution, favorably, the susceptibility to pitting corrosion decreases. This beneficial effect is ascribed to the smaller area of the alloy matrix exposed to the chloride solution with augment in particle size distribution, substantially when going from monomodal to bimodal SiC_p particle size distribution.

1. Introduction

Aluminum-matrix-composites (AMCs) reinforced with SiC particles have received considerable attention over the last three decades due to the attractive properties resulting from the combination of their constituents, such as high thermal conductivity, specific strength, tailorable coefficient of thermal expansion, improved modulus of rupture and low density. For this reason, they have been considered for applications in the aerospace, military, automotive, and electronic industries [1–3]. As for the latter, Al/SiC composites have been proposed for electronic packaging as heat sink parts in microwave housing and chip carriers. For these types of applications it is essential to increase the volume fraction of the ceramic reinforcement in excess of 50 vol.% [2]. When the Al/SiC composites are fabricated by the liquid metal infiltration route, this requirement can be met by accommodating reinforcements of different sizes into the porous ceramic preform. Therefore, particle size distribution becomes a critical parameter in process optimization.

In the continuous effort to increasingly improve the properties of Al/SiC composites, numerous investigations – with different goals – have been undertaken, including studies on the correlation between processing and microstructure, mechanical/thermal property evaluation, and, corrosion behavior studies. The latter is perhaps one of the least explored fields, particularly when dealing with composites with multimodal distribution of SiC reinforcements. It is generally accepted that pitting attack is the most common form of corrosion in Al/SiC composites. This attack can occur by the difference in corrosion potential in a local cell formed in or on the metal surface by the presence of anodic or cathodic microconstituents such as insoluble intermetallic compounds or single elements [4]. Another important degradation mechanism is due to Al_4C_3 formation by the dissolution of SiC in the molten aluminum alloy during processing. Subsequent exposure of the composites to liquid water or moisture leads to a gradual degeneration of the composites. Several approaches have been proposed and practiced to avoid formation of this deleterious phase, namely: a) additions of Si into the Al matrix [5], b) artificial oxidation to produce a SiO_2 layer on SiC [6], and c) incorporation of silica particles into the porous SiC preforms [7,8]. All these approaches can be conducive to the in situ formation or precipitation of new phases.

Regarding the role of the reinforcements in the composites' corrosion behavior, previous investigations indicate that SiC is conductive and acts as a local cathode for the reduction of oxygen [9]. This finding is in good agreement with that reported by Trowsdale et al. [10], suggesting that the susceptibility to pitting was intensified with increased SiC size. There are several previous works focused on the pitting corrosion behavior of Al/SiC composites – some of them based on continuous fiber reinforcements [4,11,12] – with high volume fraction (10 to 60 vol.%) of SiC, but with monomodal distribution of the reinforcement [9,10,13,14]. And although there are currently various reports on the mechanical properties of composites with bimodal distribution [1,2,15–18], to the authors' best knowledge, studies on the role of particle size distribution (with more than two particle sizes) and particle

* Corresponding author. Tel.: +52 844 438 9600x9678; fax: +52 844 438 9610.
E-mail addresses: martin.pech@cinvestav.edu.mx, martin_pech@yahoo.com.mx (M.I. Pech-Canul).

0032-5910/$ – see front matter © 2009 Elsevier B.V. All rights reserved.
doi:10.1016/j.powtec.2009.06.009

size ratio in the composites' corrosion behavior still remain unpublished. Understanding how SiC particle size distribution affects certain key corrosion parameters, can significantly assist to establishing a balance between high stiffness/high thermal conductivity – for instance, for electronic packaging – and corrosion performance in certain environments (for example, saline and humid ambient). The aim of this work was to investigate the effect of multimodal-size distribution (combining up to four distinct particle sizes) of SiCp reinforcements on the electrochemical behavior (pitting, passivation and corrosion potential) of Al/SiC composites fabricated by pressureless infiltration.

2. Experimental procedures

2.1. Preform preparation and characterization

The raw materials for preforms (with 40% porosity) preparation were SiC powders of four different sizes (10, 54, 86 and 146 μm average particle size) and colloidal silica. The colloidal suspension of SiO_2 (0.02–0.06 μm particle size, according to the supplier) was used as a coating on the powders to prevent attack of the SiC reinforcements by the liquid aluminum alloy during infiltration. The SiC powders were characterized by laser diffraction using a Coulter equipment. It should be pointed out that, to better control the preforms characteristics (specifically, particle size distribution and particle size ratio), the powders in the as-received condition were sieved independently, thus reducing the amplitude of the size distribution. Results from the characterization of the four sizes of powders after sieving are shown in Fig. 1.

The coating and preform preparation were carried out according to the following procedure. The silica suspension was placed in a beaker and stirred at a constant rate using a Barnant electromechanical mixer. In order to obtain a homogeneous mixture, the corresponding amounts of SiC powders, were pre-mixed manually for 5 min in a porcelain mortar. Such amounts were determined based on the density of SiC and characteristics of each of the preforms, i.e., SiC volume fraction and particle size distribution (monomodal, bimodal, etc). Then, the pre-mixed powders were added gradually to the suspension during the stirring, while the system was heated at 50 °C in a Cimarec hot-plate-stirring system for 30 min. Fig. 2 shows representative photomicrographs of uncoated and coated SiC particles. Finally, after drying the mixture in an air forced drier at ~200 °C for 2 h, the powders were placed into a steel mold and compacted uniaxially (~3.5 MPa) using a hydraulic press to produce plate-shaped preforms of 3 cm × 4 cm × 0.5 cm with 40% porosity. In order to show the distribution of SiC powders after pre-mixing, the mixtures were characterized by laser diffraction as well. The results presented in Fig. 3 show that in each of the four graphs, one can distinguish the number of peaks according to the respective distribution.

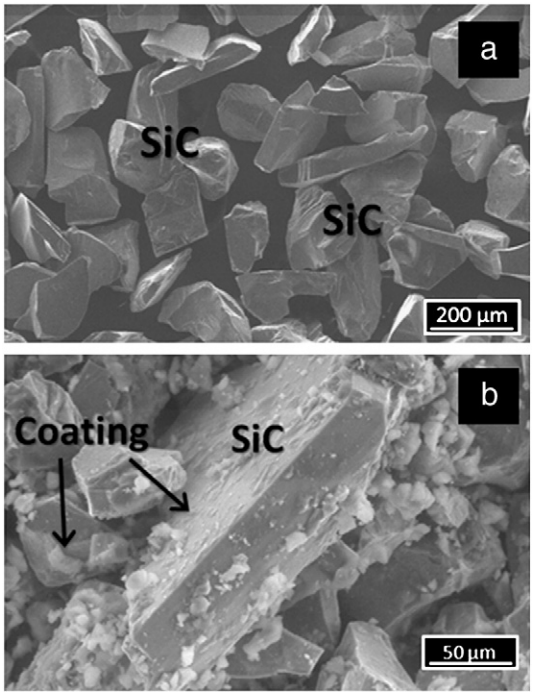

Fig. 2. Representative SEM photomicrographs of: a) uncoated and b) silica-coated SiC particles.

Preforms with monomodal, bimodal, trimodal, and cuatrimodal size distribution, with 1, 1:5, 1:1:4 and 1:1:1:3 particle size ratios, respectively, were prepared with 0.60 volume fraction of ceramic material (0.5 vol. fraction α-SiC + 0.1 vol. fraction of SiO_2 in the form of

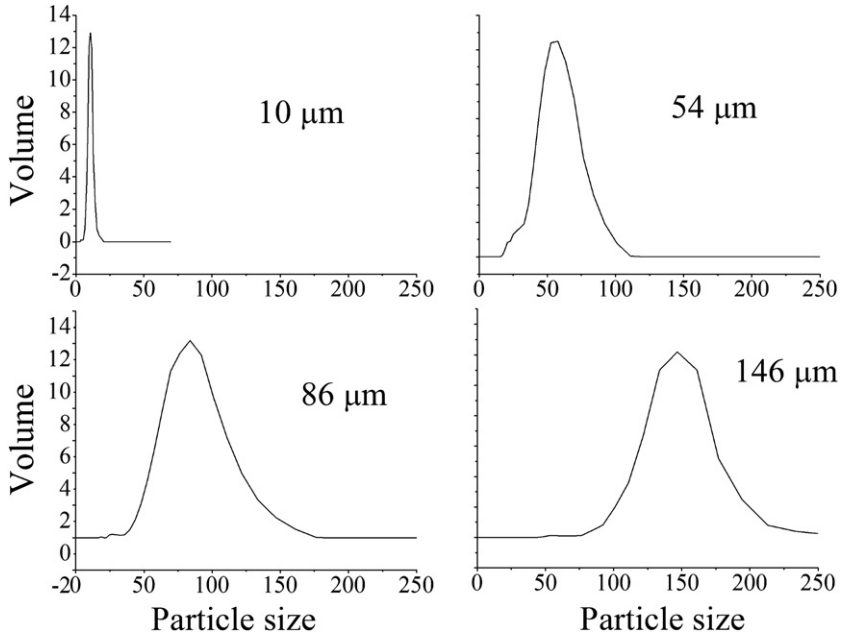

Fig. 1. Particle size distribution for each of the sieved powders used in the experiment.

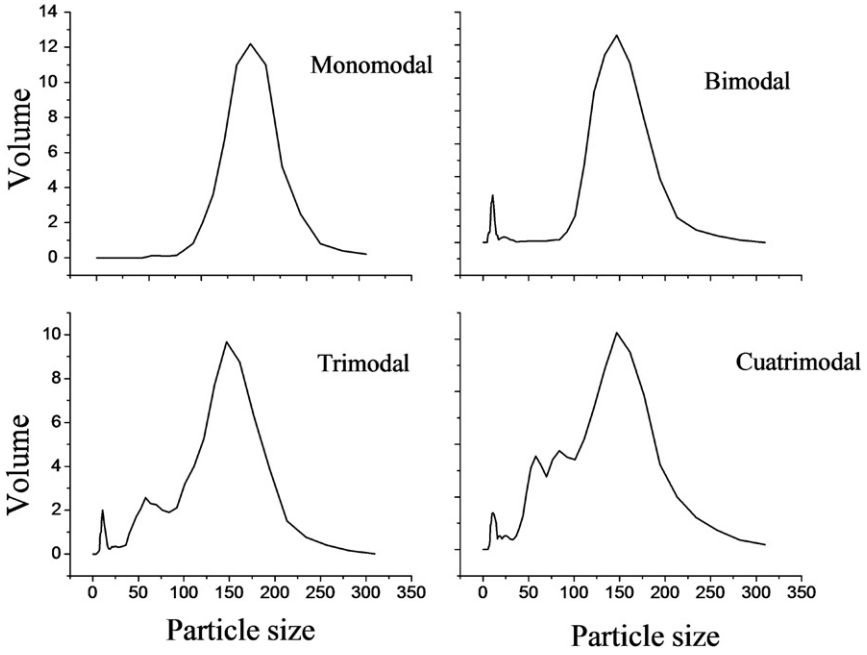

Fig. 3. Graphs of the distributions of SiC mixed powders for the preparation of preforms with monomodal, bimodal, trimodal and cuatrimodal distributions.

coatings on the SiC particles), according to the abovementioned procedure. In this context, particles of 10, 54, 86 and 146 μm are referred to as small, medium-1, medium-2, and large, correspondingly. Particle size ratio designation involves both, the preform type (monomodal, bimodal, trimodal, and cuatrimodal) and the proportion of each particle size. Systematically, bimodal, trimodal, and cuatrimodal preforms consist of small/large, small/medium-1/large and small/medium-1/medium-2/large particles, respectively. For instance, 1:5 represents a bimodal preform prepared with one part of small particles and five parts of large ones; 1:1:1:3 stands for a cuatrimodal preform made up of one part of small particles, one part of medium-1 particles, one part of medium-2 particles, and three parts of large ones. Monomodal preforms are just designated with the corresponding particle size; for this particular case, the particle size was 146 μm.

With the aim of determining pore size, the preforms were mounted in epoxy resin, ground, and polished using standard procedures. Subsequently, the specimens were photographed in backscattered mode using a Philips XL30 ESEM scanning electron microscope at an excitation voltage of 20 KV and working distance between 10 and 15 mm. In order to determine the average pore size in each type of preform, and with the aid of an image analyzer (Image Pro Plus software), at least 15 pore size measurements were carried out per specimen mounted in

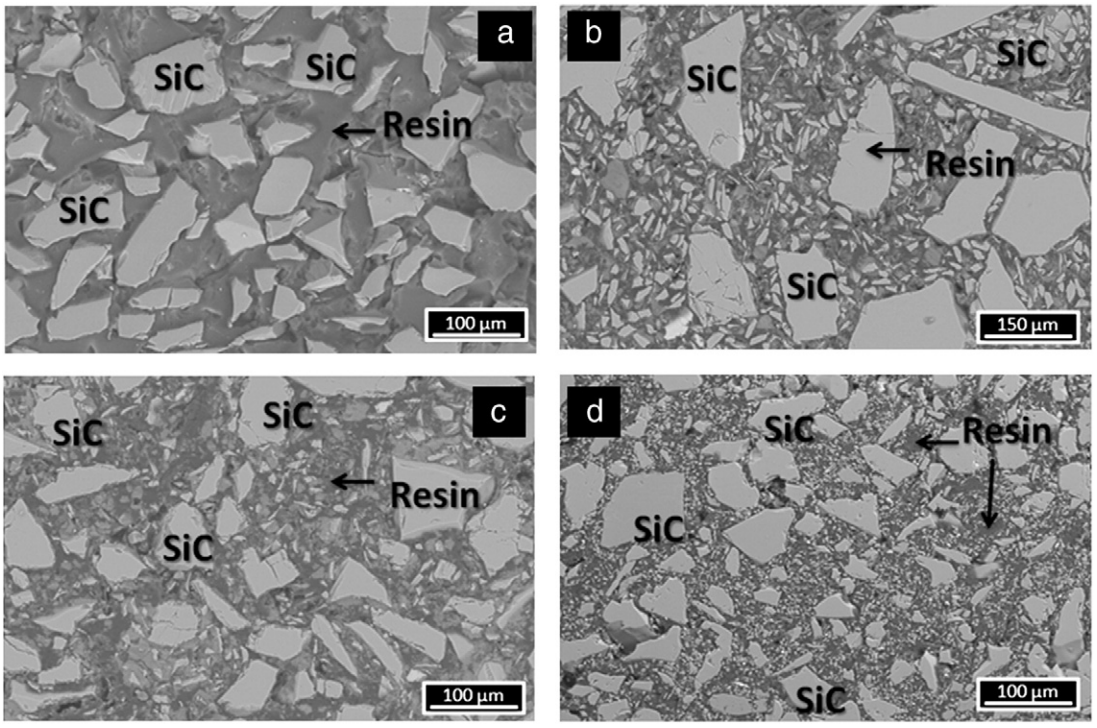

Fig. 4. Representative SEM photomicrographs of SiC preforms mounted in epoxy resin. Specimens in these conditions were used for pore size measurements using an image analyzer.

Table 1
Chemical composition of commercial aluminum and the fabricated alloy (wt.%).

	Al	Mg	Si	Fe	Mn	Cu	Si/Mg
Commercial aluminum	98.22	0.23	0.12	1.28	0.110	0.04	–
Alloy	84.13	13.29	1.78	0.626	0.118	0.055	0.116

resin. Representative photomicrographs of mounted specimens for pore size measurements are shown in Fig. 4.

2.2. Composites fabrication

The aluminum alloy used in the investigation was fabricated from Al of commercial purity with additions of Mg and Si, in an induction furnace with a capacity of 10 kg. Previous to casting in a metallic mold, the alloy was degassed at 680 °C using argon gas for 10 min. The chemical compositions of commercial purity Al and of the aluminum alloy are given in Table 1. The composites were fabricated by infiltrating the aluminum alloy Al–13 Mg–1.8Si (wt.%) – purposely designed for the current investigation – into the ceramic preforms in a horizontal tube furnace with a 6.5 cm diameter alumina tube closed at both ends with end-cap fittings to control the process atmosphere. The preform and approximately 32 g of the alloy were placed in a ceramic container and the whole assembly was positioned in the tube center. The system was heated at a rate of 15 °C/min up to 1100 °C, held at that temperature for 60 min and then cooled down with the same rate to room temperature. During the heating period and up to 1000 °C, the specimens were treated in ultra high purity (UHP) argon. Then, in order to enhance the wetting of the preform by the liquid alloy, a change in the atmosphere from Ar to UHP N_2 was conducted at 1000 °C.

2.3. Composites characterization and electrochemical tests

Once the system was cooled down to room temperature, the composite specimens were prepared for microstructure characterization using X-ray diffraction (XRD), scanning electron microscopy (SEM)) and energy dispersive X-ray spectroscopy (EDS). Additionally, electrochemical tests were performed on the composites. XRD tests were performed using a Philips-3040 diffractometer (Cu-K_α monochromatic radiation) at a scanning rate of 0.02 °/s, from 15 to 80 2θ°; the excitation voltage and current were of 40 KeV and 30 mA, respectively. SEM analysis was conducted in a JEOL JSM 6300 scanning electron microscope in the backscattered electron mode at a working distance between 10–15 mm, and acceleration voltage of 20 KV. Cyclic polarization tests were performed using a Gamry CNS 100/PC3 potentiostat. In preparation for the electrochemical tests, the specimens were sectioned to an exposed area of 10 mm × 10 mm, mounted carefully in epoxy resin to avoid crevice conditions, and ground with 80–1200 grit SiC abrasive paper. The specimens were then polished manually using diamond suspensions from 3 to 1/10 μm in Buehler nylon cloths, and finally, with silica gel in chemomet Buehler clothes. The electrochemical tests were carried out using a 0.1 M NaCl de-aerated solution in a Pyrex glass cell, with a three-electrode set-up. Accordingly, a saturated calomel reference electrode (SCE) and a platinum counter electrode were used, with the analyzed specimen as working electrode. With the aim of accurately establishing the corrosion (E_{corr}) and pitting (E_{pit}) potentials, the electrodes were initially allowed to stabilize at their corrosion potentials (E_{corr}) in de-aerated solutions, by passing nitrogen gas (N_2) through the solution before and during the measurements. Subsequently, the electrodes were polarized in the electropositive direction at a scanning rate of 0.333 V/s, starting at −1.4 V until the potential reached the value of −0.3 V, after which the scan direction was reversed to finish at the starting point value, −1.4 V. Thermodynamic calculations on the feasibility of certain chemical reactions involved were performed using the FactSage® program and databases.

3. Results and discussion

3.1. Microstructure characterization

Results from pore size measurements indicate that the average pore size for monomodal, bimodal, trimodal and cuatrimodal distributions are 22.53 ± 2.65, 7.74 ± 1.3, 6.99 ± 1.24, and 6.55 ± 1.24 μm, respectively. It is clear that pore size drops by about 65% from monomodal to bimodal; then, from bimodal to trimodal and cuatrimodal, the decrease is less significant. This outcome is explained by the accommodation of the small and medium particles in the space left by the large particles. It should be recalled that the pores in the ceramic preforms are filled out by the aluminum alloy during the infiltration process.

Results from the characterization by X-ray diffraction before and after the electrochemical tests showed the presence of the same phases (Mg_2Si, $MgAl_2O_4$, MgO and AlN) in addition to Al, Si and SiC from the starting material. Figs. 5 and 6 show typical diffractograms corresponding to composites with monomodal, bimodal, trimodal, and cuatrimodal distributions, before and after the electrochemical tests, respectively. According to thermodynamics and previous works [6,7,19,20], silica reacts with the aluminum alloy (in the presence of Mg), giving place to the formation of spinel and magnesium oxide. In this particular investigation, since silica is forming coatings on the SiC particles, the abovementioned interactions avoid the attack of the SiC particles by the molten alloy and in consequence, successfully avoided

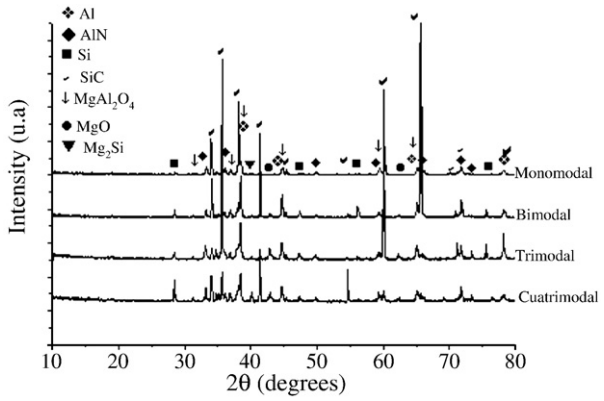

Fig. 5. Representative diffractograms of Al/SiC composites with monomodal, bimodal, trimodal and cuatrimodal distributions before the electrochemical tests.

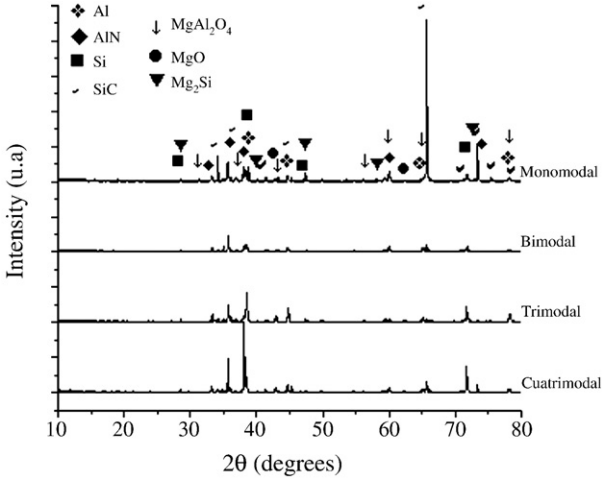

Fig. 6. Representative diffractograms of Al/SiC composites with monomodal, bimodal, trimodal and cuatrimodal distributions after the electrochemical tests.

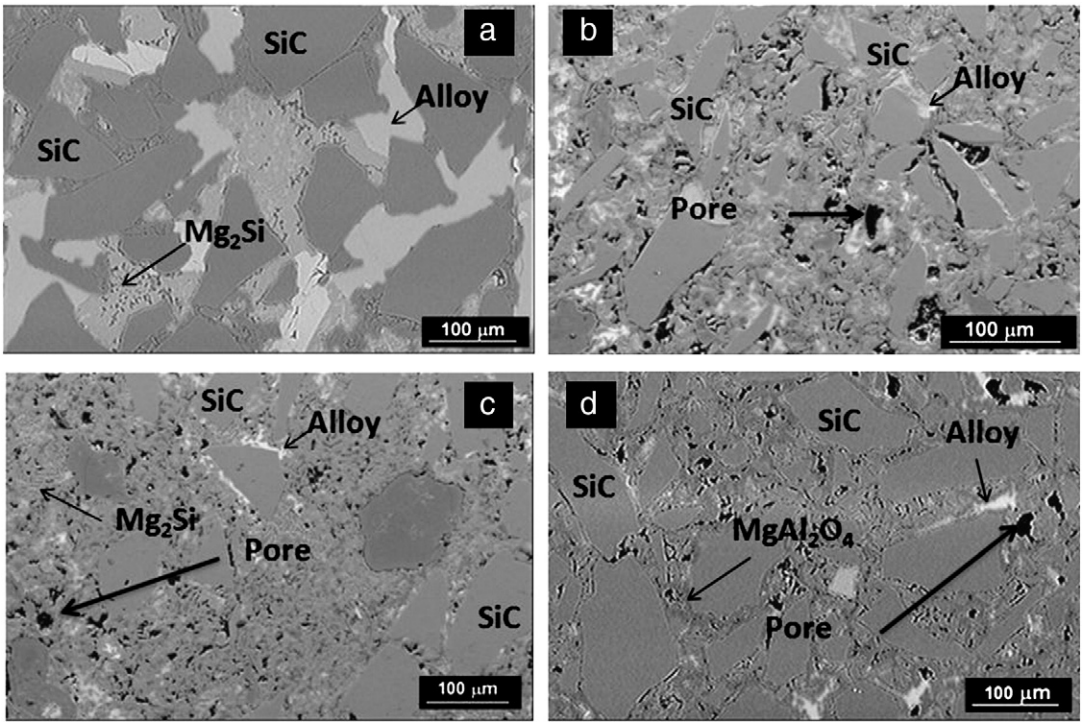

Fig. 7. Typical microstructure of Al/SiC composites with a) monomodal, b) bimodal, c) trimodal and d) cuatrimodal distributions.

formation of the undesirable Al_4C_3 phase in the composites. The spinel, magnesium oxide, magnesium silicide, and aluminum nitride phases are formed in situ during processing according to:

$$2Al_{(1)} + Mg_{(1)} + 2SiO_{2(s)} = MgAl_2O_{4(s)} + 2Si_{(s)} \quad (1)$$

$$\Delta G_{1100\,^{\circ}C} = -484\,\text{kJ/mol}$$

$$\Delta H_{1100\,^{\circ}C} = -388\,\text{kJ/mol} \quad (2)$$

$$2Mg + SiO_2 = 2MgO + Si$$

$$\Delta G_{1100\,^{\circ}C} = -253.04\,\text{kJ/mol}$$

$$\Delta H_{1100\,^{\circ}C} = -295.7\,\text{kJ/mol}$$

The presence of the AlN in the microstructure is explained through the reaction of molten aluminum and nitrogen gas according to [21]:

$$Al\,(1) + [N] = AlN_{(S)} \quad (3)$$

$$\Delta G_{1100\,^{\circ}C} = -328\,\text{kJ/mol}$$

Moreover, due to its lower vaporization temperature as compared with that for aluminum at normal pressure, magnesium escapes from the melt during processing. Previous reports indicate that Mg in vapor phase reacts with nitrogen and returns to the alloy according to the following reactions [22]:

$$3Mg_{(g)} + 2N_{(g)} \rightarrow Mg_3N_{2(s)} \quad (4)$$

$$\Delta G_{1100\,^{\circ}C} = -90.70\,\text{kJ/mol}$$

$$\Delta H_{1100\,^{\circ}C} = -183.03\,\text{kJ/mol}$$

$$2Al_{(l)} + Mg_3N_{2(s)} \rightarrow 2AlN_{(s)} + 3\,mg_{(g)} \quad (5)$$

$$\Delta G_{1100\,^{\circ}C} = -167.82\,\text{kJ/mol}$$

$$\Delta H_{1100\,^{\circ}C} = -218.22\,\text{kJ/mol}$$

The net effect of the recycling process – represented by Eqs. (4) and (5) – is to enhance the wettability of silicon carbide by the Al–Mg–Si alloy. The wetting enhancement mechanism has been extensively reported in the previous literature [7,21,22]. The analysis by XRD also showed that the type of phases formed in situ is not influenced by particle size distribution, because the same phases were formed in all the four kinds of composites. This in turn, is due to the protection provided by the silica coating.

Fig. 7(a)–(d) shows typical microstructures of the composites – of polished specimens – with monomodal, bimodal, trimodal, and cuatrimodal distribution, respectively, before the electrochemical tests. In the typical microstructure of the composites, it is observed that the SiC particles do not seem to be attacked by the aluminum alloy and that they are surrounded by the spinel phase. This fairly explains the soundness of the reinforcements and the absence of the unwanted aluminum carbide. It should be noted, however, that the composites exhibit some degree of porosity before the electrochemical tests. Fig. 8a shows a representative microstructure of composites after the electrochemical test, in which, it is observed that most of the alloy is attacked, with the corrosion products having sponge-like morphology. Fig. 8b is a magnification of the selected region shown in Fig. 8a. According to EDS analysis (representative spectrum also shown in Fig. 8b), the corrosion products have high contents of O, Al, Mg and Si. These elements suggest the presence of aluminum hydroxide ($Al(OH)_3$), magnesium hydroxide ($Mg(OH)_2$) and hydrated silica ($SiO_2{\cdot}nHO_2$). In order to verify the presence of hydroxides in the corrosion products, representative samples were collected from the surface of the composites and analyzed by Fourier Transformed Infrared Spectroscopy (FTIR), using a Nicolet Avatar 360 equipment, with 64 scans per spectrum in the absorption mode. The results show a signal band from 3500 to 3700 cm^{-1}, which in accordance with the literature, falls within the band corresponding to OH^- group (3200−3700 cm^{-1}). The remaining signals correspond to Si–O–Si and Al–O–Si bonds, related to the spinel and residual silica [23,24]. Fig. 9 is a representative FTIR spectrum of the corrosion products. The analysis and the physicochemical characteristics of the corrosion products confirm the presence of aluminum hydroxide and magnesium hydroxide.

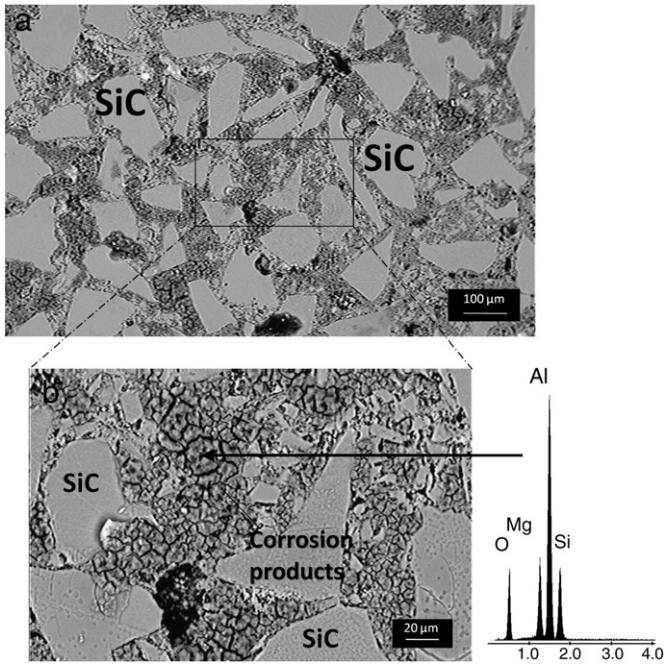

Fig. 8. a) Representative photomicrograph of composite after cyclic polarization test. Corrosion products are observed on the composites surface; b) is a magnification of the selected region shown in panel a.

3.2. Electrochemical measurements

3.2.1. Cyclic polarization

Fig. 10 shows cyclic polarization curves obtained in the electrochemical tests. Fig. 10a is for composites with monomodal and bimodal distributions respectively, while Fig. 10b pertains to composites with trimodal and cuatrimodal distributions, correspondingly. In all the curves, the corrosion (E_{corr}) and passivation (E_{pass}) potentials are distinctly defined, in the ranges −1.34 to −1.37 V and −0.93 to −1.01, respectively. Above E_{corr}, a relatively constant region in the current density (between 10^{-6} and 10^{-5} A/cm^2) is observed; this region has been associated to the formation of a passive layer on the aluminum alloy. Increasing the applied voltage allows reaching the pitting potential (E_{pit}), in the range of −0.56 to −0.65 V. After this point, current density increases continuously with voltage. This behavior, on the other hand, has been attributed to the rupture of the passive layer [10]. Table 2 presents the electrochemical parameters for each of the composites with different particle size distributions tested. E_{pit} values are −0.65, −0.56, −0.63 and −0.60 V for monomodal, bimodal, trimodal, and cuatrimodal distributions, respectively. It is evident that the pitting potentials become less negative (more noble behavior) with increase in particle size distribution. The notable decrease in E_{pit} from monomodal to bimodal and the subsequent increase for tri- and cuatrimodal distribution isn't clear yet, and requires a more detailed investigation. It is well known that the more electropositive the magnitude of E_{pit}, the greater the resistance of the passive layer to the attack by chloride ions, because a higher potential would be required to induce pitting. From Fig. 4 and from pore size measurements – within the framework of the current experiment – it is evident that higher SiC particle size distributions yield smaller Al-alloy areas (substantial decrease from monomodal to bimodal) exposed to the chloride solution, thus diminishing the alloy susceptibility to pitting nucleation and growth.

Moreover, the resistance of the passive layer can be related to the decrease in the residual porosity of the composite, because – as observed in the current work – increasing particle size distribution leads to a decrement in residual porosity (see Table 2). As it is well known, the higher the porosity, the higher the number of sites for localized

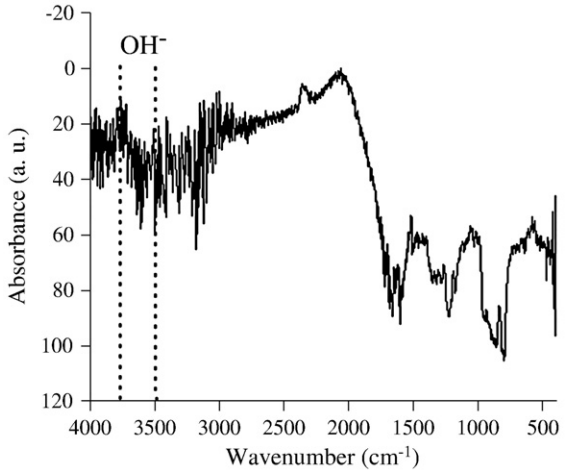

Fig. 9. FTIR spectrum of corrosion products collected from the surface of the composites.

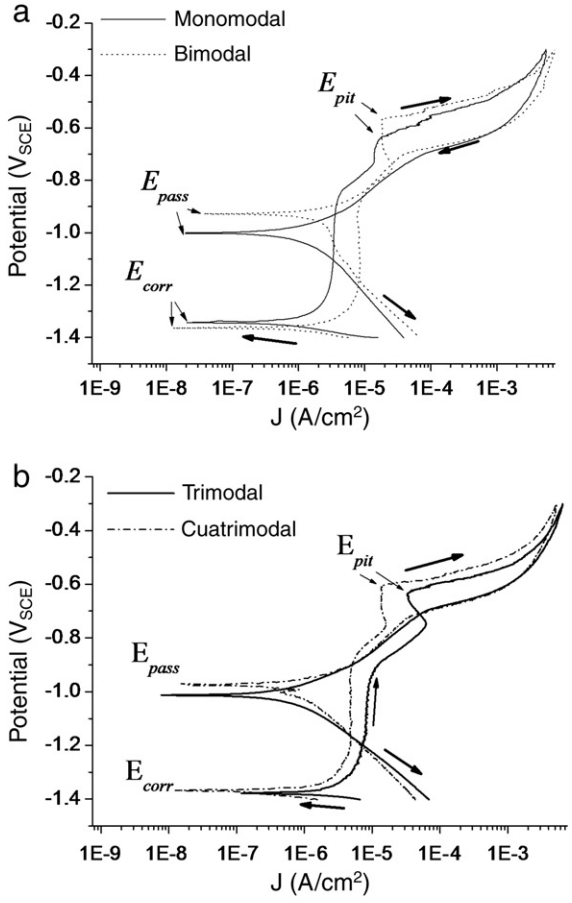

Fig. 10. Typical polarization curves for composites with (a) monomodal and bimodal distribution, and (b) trimodal and cuatrimodal distributions.

Table 2
Density, porosity and corrosion parameters of composites with multimodal distributions.

Distribution	E_{corr} (V_{SCE})	E_{pit} (V_{SCE})	E_{pass} (V_{SCE})	Density (g/cm^3)	Residual porosity (%)
Monomodal	−1.34	−0.65	−1.00	2.84	4.42
Bimodal	−1.36	−0.56	−0.93	2.92	1.49
Trimodal	−1.37	−0.63	−1.01	2.93	1.40
Cuatrimodal	−1.36	−0.60	−0.97	2.96	0.49

attack. It should be noticed however, that as reported in previous works studying the effect of particle size on the pitting behavior [10], the measured pitting potentials in this investigation compare favorably because a difference of about 40 mV in the electropositive direction is observed. Another and more useful approach to understand this effect is by the difference between E_{pit} and E_{corr}, since its magnitude provides an insight into the easiness or difficulty with which pitting can occur; the larger the magnitude of $E_{pit} - E_{corr}$, the greater the difficulty to induce pitting. Interestingly, the smallest and largest differences are for monomodal and cuatrimodal distributions, respectively.

4. Summary and conclusions

The effect of coated-SiC_p multimodal-size-distribution on the pitting behavior of Al/SiC_p composites has been investigated. The composites were fabricated by the liquid infiltration of performs prepared with silica-coated SiC particles in monomodal, bimodal, trimodal and cuatrimodal fashion. Accordingly, the composites were characterized electrochemically measuring the passivation, corrosion and pitting potentials. As expected, the SiO_2 coatings helped to successfully protect the SiC particles and avoid formation of the unwanted Al_4C_3 phase. A detailed characterization of the corrosion products in the composites after the electrochemical tests confirms the presence of aluminum hydroxide and magnesium hydroxide. Pitting corrosion potential, E_{pit}, becomes less negative (more noble or in the electropositive direction) with increase in particle size distribution. The corresponding values for monomodal, bimodal, trimodal and cuatrimodal distribution are −0.65, −0.56, −0.63 and −0.60 V, respectively. This behavior is associated to the higher resistance of the passive layer to rupture by the action of chlorides, which is ultimately interpreted as higher potential required to induce the pitting on the aluminum matrix. On the other hand, – within the framework of the current study– E_{corr} and E_{pass}, don't seem to be influenced by particle size distribution.

Acknowledgements

Mr. M. Montoya-Dávila gratefully acknowledges Conacyt (National Council of Science and Technology, in México) for providing a doctoral scholarship. Authors also thank Mrs. M. Echeverría for her technical assistance during the electrochemical tests performed at Cinvestav-Merida. Mrs. M. Rivas-Aguilar and Mr. S. Rodriguez-Arias are also thanked for their technical assistance during the characterization by SEM and XRD, respectively.

References

[1] Y. Cui, High volume fraction SiC/Al composites prepared by pressureless melt infiltration: processing, properties and applications, Key Engineering Materials 249 (2003) 45–48.
[2] H.S. Lee, C.S. Lee, J.R. Lee, Pressure infiltration casting process and thermal properties of high volume fraction SiC_p/Al composites for electronic packaging, Aluminum Transactions 3 (1) (2000) 1–6.
[3] A. Pardo, M.C. Merino, S. Merino, F. Viejo, M. Carboneras, R. Arrabal, Influence of reinforcement proportion and matrix composition on pitting corrosion behaviour of cast aluminium matrix composites (A3xx.x/SiCp, Corrosion Science 47 (2005) 1750–1764.
[4] S.L. Winkler, M.P. Ryan, H.M. Flower, Flower, Pitting corrosion in cast 7XXX aluminium alloys and fiber reinforced MMC´s, Corrosion Science 46 (2004) 893–902.
[5] J.C. Lee, J.Y. Byun, S.B. Park, H.I. Lee, Prediction of Si contents to suppress the formation of Al_4C_3 in the SiC_p/Al composite, Acta Materialia 46 (5) (1998) 1771–1780.
[6] Z. Shi, S. OChiai, M. Hojo, J. Lee, M. Gu, H. Lee, Joining characteristics of oxidized SiC particles reinforced Al-Mg matrix composite prepared by reaction infiltration processing, Journal of Material Research 16 (2) (2001) 400–406.
[7] M. Rodriguez Reyes, M.I. Pech Canul, J.C. Rendón Angeles, J. López Cuevas, Limiting the development of Al_4C_3 to prevent degradation of Al/SiCp composites processed by pressureless infiltration, Composites Science and Technology 66 (8) (2006) 1056–1062.
[8] M. Montoya, M.A. Pech Canul, M.I. Pech Canul, Microstructure and mechanical properties of Al/SiCp composites with multimodal size distribution of reinforcements, Materials Science Forum 560 (2007) 115–120.
[9] L. Díaz Ballote, L. Veleva, M.A. Pech Canul, M.I. Pech Canul, O. Wipf David, Activity of SiC particles in Al-based metal matrix composites revealed by SECM, Journal of the Electrochemical Society 151 (6) (2004) 299–303.
[10] A.J. Trowsdale, B. Noble, S.J. Harris, I.S.R. Gibbins, G.E. Thompson, G.C. Wood, The influence of silicon carbide reinforcement on the pitting behaviour of aluminium, Corrosion Science 38 (2) (1996) 177–191.
[11] C.R. Crowe, Corrosion behavior of SiC/Al metal matrix composites, Journal of Electrochemical Society 130 (9) (1983) 1804–1809.
[12] P.P. Trzaskoma, Pit morphology of aluminum alloy and silicon carbide/aluminum alloy metal matrix composites, Corrosion 46 (5) (1990) 402–409.
[13] S. Candan, E. Bilgic, Corrosion behavior of Al-60 vol.% SiCp composites in NaCl solution, Materials Letters 58 (2004) 2787–2790.
[14] G.E. Kiourtsidis, S.M. Skolianos, Pitting corrosion of artificially aged T6 AA2024/SiCp composites in 3.5 wt.% NaCl aqueous solution, Corrosion Science 49 (2007) 2711–2725.
[15] C.W. Nan, D.R. Clarke, The influence of particle size and particle fracture on the elastic/plastic deformation of metal matrix composites, Acta Materialia 44 (9) (1996) 3801–3811.
[16] C.Y. Chen, C.G. Chao, Effect of particle-size distribution on the proprieties of high volume-fraction SiC_p-Al-based composites, Metallurgical and Materials Transactions A 31A (2000) 2351–2359.
[17] R. Arpón, Molina J.M, Saravanan R A, García-Cordovilla C, Louis E, Narciso J. Thermal expansion behavior of aluminum/SiC composites with bimodal particle distributions, Acta Materialia 51 (2003) 3145–3156.
[18] M. Montoya-Dávila, M.A. Pech-Canul, M.I. Pech-Canul, Effect of bi- and trimodal size distribution on the superficial hardness of Al/SiCp composites prepared by pressureless infiltration, Power Technology 76 (2007) 66–71.
[19] A.D. McLeod, C.M. Gabryel, Kinetics of growth of spinel, $MgAl_2O_4$, on alumina particulate in aluminum alloys containing magnesium, Metallurgical Transactions A 23A (1992) 1279–1283.
[20] B.C. Pai, Ramani Geetha, R.M. Pillai, K.G. Satyanarayana, Role of magnesium in cast aluminum alloy matrix composites, Journal of Materials Science 30 (1995) 1903–1911.
[21] Q. Hou, R. Mutharasan, M. Koczak, Feasibility of aluminum nitride formation in aluminum alloys, Materials Science and Engineering 195A (1995) 121–129.
[22] M.I. Pech Canul, R.N. Katz, M.M. Makhlof, The combined role of nitrogen and magnesium in wetting SiC by aluminum alloys, XXII International Congress of Metallurgy and Materials, Held in Saltillo Coahuila, México, November 8–10 (2000) 232–241.
[23] R. Escalera-Lozano, C.A. Gutierrez, M.A. Pech-Canul, M.I. Pech Canul, Degradation of Al/SiC composites produced with rice-hull ash and aluminum cans, Waste Management 28 (2008) 389–395.
[24] W.K.W. Lee, J.S.J. Van Deventer, Use of infrared spectroscopy to study geopolymerization of heterogeneous amorphous aluminosilicates, Langmuir 19 (2003) 8726–8734.